

# Dynamics of phase separation in two species Bose-Einstein condensates with vortices

Soumik Bandyopadhyay,<sup>1,2</sup> Arko Roy,<sup>1</sup> and D. Angom<sup>1</sup>

<sup>1</sup>*Physical Research Laboratory, Ahmedabad - 380009, Gujarat, India*

<sup>2</sup>*Indian Institute of Technology Gandhinagar, Gandhinagar - 382424, Gujarat, India*

(Dated: February 28, 2017)

We examine the dynamics associated with the miscibility-immiscibility transition of trapped two-component Bose-Einstein condensates (TBECs) of dilute atomic gases in presence of vortices. In particular, we consider TBECs of Rb hyperfine states, and Rb-Cs mixture. There is an enhancement of the phase-separation when the vortex is present in both condensates. In the case of a singly charged vortex in only one of the condensates, there is enhancement when the vortex is present in the species which occupy the edges at phase-separation. But, suppression occurs when the vortex is in the species which occupies the core region. To examine the role of the vortex, we quench the inter-species interactions to propel the TBEC from miscible to immiscible phase, and use the time dependent Gross-Pitaevskii equation to probe the phenomenon of phase-separation. We also examine the effect of higher charged vortex.

PACS numbers: 67.85.d, 67.40.Vs, 67.57.Fg, 67.57.De

## I. INTRODUCTION

Miscibility-immiscibility phase transition in a TBEC of dilute atomic gases, is a novel quantum phenomenon. It is also referred to as phase-separation, and provides a scheme to understand the physics governing a wide range of processes such as pattern formation, nonlinear excitations, dynamical and interface instabilities [1–3]. Further more, it is the key to gain insights on phenomena such as quantum phase transition and criticality, symmetry breaking phenomena, Kibble-Zurek mechanism [4], collective modes [?] etc. In experiments, TBECs consisting of two different atomic species [5–11], different isotopes of the same atomic species [12, 13] or two different hyperfine spin states [14–16] have been realized. During the past two decades numerous theoretical studies have examined the static [17, 18] and dynamical properties of phase-separation [19–21]. From these studies it is clear that in the Thomas-Fermi (TF) limit at zero temperature the relative values of the intra and inter-species interactions determine the miscibility or immiscibility of the condensates. The condition for the phase-separation is the inequality  $g_{12} > \sqrt{g_{11}g_{22}}$ , where  $g_{12}$  is the inter-species interaction strength, and  $g_{kk}$  is the intra-species interaction of the  $k$ th species. Based on this the TBEC can be driven from one phase to other by tuning the interaction strengths. However, an important point to be noted is that the derivation of the inequality assumes the TBEC to be in the ground state, that is, in absence of topological defects and impurities in the condensates. This aspect requires due investigation as there can be deviations from the inequality when vortices are present in the condensates. The effects of finite temperature on the dynamics of miscibility-immiscibility phase-separation of a TBEC is a topic of recent interest [21]. In addition, suppression of phase-separation of a TBEC at finite temperatures has been reported [22]. It has also been shown in theoretical investigations that inclusion of kinetic energy terms in the total energy expression of a TBEC, results in partial or complete suppression of phase-separation [23]. This is to be contrasted with the TF approximation where the kinetic energy term is neglected.

In this work we theoretically investigate the effect of vortices on the dynamics of phase-separation in TBECs. An obvious way in which the vortices can influence the dynamics of phase-separation is through the centrifugal force arising from the associated superfluid flow. Thus, depending on the species in which vortex is introduced there can either be enhancement or suppression of phase-separation. In terms of experimental realizations, vortex in TBECs may be produced using the method of phase imprinting [24, 25], stirring of the condensates by Gauss-Laguerre laser beams [26], rotating the trapping potential [27, 28], through evaporative cooling process [29] or by interconversion between the two components of in the case of a TBEC with two hyperfine states [30]. Other than the effects on the dynamics of phase separation, vortices in condensates are topological defects which are essential ingredient of several novel phenomena. For the present work we examine the effects of when a vortex is present in one of the condensate species in a TBEC, as well as vortices are present in both the species. In addition, we also investigate the effects of the charge of the vortex, and it is expected that higher charged vortices shall have a larger effect. However, equally important is the dynamics and stability associated with a vortex with higher charge or vorticity.

The paper is organized as follows. In Sec. II we formulate the dynamics of phase-separation of a TBEC at zero temperature, in the Gross-Pitaevskii framework, and discuss on the effects of centrifugal force associated with vortex induced superfluid flows in the condensates. Sec. III provides a brief description of the numerical schemes used to probe the phenomenon of phase-separation, and investigate on the dynamics associated with it. In Sec. IV, we present the results describing the vortex induced enhancement or suppression in miscibility-immiscibility transition of the TBECs depending on its presence in the species. We also report the results from our further investigations on the dynamics in the presence of higher charged vortex. We conclude with the key highlights of our finding in Sec. V.

## II. THEORETICAL METHODS

In mean field approximation, the time evolution of the order parameters of an interacting, trapped TBEC system at  $T = 0\text{K}$ , are governed by a pair of coupled Gross-Pitaevskii (GP) equations

$$\left[ -\frac{\hbar^2}{2m_k} \nabla^2 + V_k(\mathbf{r}) + \sum_{j=1}^2 g_{kj} |\Psi_j(\mathbf{r}, t)|^2 \right] \Psi_k(\mathbf{r}, t) = i\hbar \frac{\partial \Psi_k(\mathbf{r}, t)}{\partial t}, \quad (1)$$

where,  $k = 1, 2$  is species index,  $\Psi_k$  is the condensate wave-function of the  $k$ th species, and  $V_k(\mathbf{r})$  is the trapping potential. The intra and inter-species interaction strengths are given by  $g_{kk} = 4\pi\hbar^2 a_{kk}/m_k$ , and  $g_{kj} = 2\pi\hbar^2 a_{kj}/m_{kj}$ , respectively. Here,  $a_{kk}$  and  $a_{kj}$  are the intra and inter-species  $s$ -wave scattering lengths of atoms,  $m_k$  is mass of the  $k$ th species, and  $m_{kj} = m_k m_j / (m_k + m_j)$  is the reduced mass. The order parameters or wave functions of each of the species are normalized to the total number of atoms in the condensates

$$N_k = \int d\mathbf{r} |\Psi_k(\mathbf{r})|^2. \quad (2)$$

With these considerations and definitions, the total energy of the TBEC system is

$$E = \int d\mathbf{r} \left[ \sum_{k=1}^2 \left( \frac{\hbar^2}{2m_k} |\nabla \Psi_k(\mathbf{r})|^2 + V_k(\mathbf{r}) |\Psi_k(\mathbf{r})|^2 + \frac{g_{kk}}{2} |\Psi_k(\mathbf{r})|^4 \right) + g_{12} |\Psi_1(\mathbf{r})|^2 |\Psi_2(\mathbf{r})|^2 \right], \quad (3)$$

where  $V_k$  is taken to be harmonic oscillator potential which is of the form

$$V_k(\mathbf{r}) = V_k(x, y, z) = \frac{1}{2} m_k \omega_k^2 (x^2 + \alpha_k^2 y^2 + \lambda_k^2 z^2). \quad (4)$$

Here,  $\omega_k$  is frequency of the trap along  $x$  direction,  $\alpha_k, \lambda_k$  are the anisotropy parameters. For the present study, we consider the atoms of both species to be trapped in the same potential, that is,  $\omega_1 = \omega_2 = \omega_x$ ,  $\alpha_1 = \alpha_2 = \alpha = \omega_y/\omega_x$ , and  $\lambda_1 = \lambda_2 = \lambda = \omega_z/\omega_x$ . Furthermore, we define the oscillator length to be  $a_{\text{osc}} = \sqrt{\hbar/(m_1 \omega_x)}$ , and energy quanta  $\hbar\omega_x$  which correspond to convenient length and energy scale of the system. To render the coupled GP equations in dimensionless form, we scale the co-ordinates to  $\tilde{x} = x/a_{\text{osc}}$ ,  $\tilde{y} = y/a_{\text{osc}}$ ,  $\tilde{z} = z/a_{\text{osc}}$ , time to  $\tilde{t} = t\omega_x$ , and total energy to  $\tilde{E} = E/(\hbar\omega_x)$ . The order parameters then follow the transformations

$$\Phi_k(\tilde{x}, \tilde{y}, \tilde{z}) = \sqrt{\frac{a_{\text{osc}}^3}{N_k}} \Psi_k(x, y, z). \quad (5)$$

Defining  $m_r = m_1/m_2$ , the total energy in Eq. (3) in dimensionless form is

$$\tilde{E} = \int d\tilde{x} d\tilde{y} d\tilde{z} \left\{ \frac{N_1}{2} \left[ |\nabla \Phi_1|^2 + (\tilde{x}^2 + \alpha^2 \tilde{y}^2 + \lambda^2 \tilde{z}^2) |\Phi_1|^2 + N_1 \tilde{g}_{11} |\Phi_1|^4 \right] + \frac{N_2}{2} \left[ m_r |\nabla \Phi_2|^2 + \frac{1}{m_r} (\tilde{x}^2 + \alpha^2 \tilde{y}^2 + \lambda^2 \tilde{z}^2) |\Phi_2|^2 + N_2 \tilde{g}_{22} |\Phi_2|^4 \right] + N_1 N_2 \tilde{g}_{12} |\Phi_1|^2 |\Phi_2|^2 \right\} \quad (6)$$

where,  $\tilde{g}_{11} = 4\pi a_{11}/a_{\text{osc}}$ ,  $\tilde{g}_{22} = m_r 4\pi a_{22}/a_{\text{osc}}$  and  $\tilde{g}_{12} = 2\pi(m_1 + m_2)a_{12}/m_2 a_{\text{osc}}$ . For notational convenience, here after we drop the tilde from the transformed quantities. The scaled coupled GP equations can then be expressed as

$$\left[ -\frac{1}{2} \nabla^2 + \frac{1}{2} (x^2 + \alpha^2 y^2 + \lambda^2 z^2) + \sum_{j=1}^2 G_{1j} |\Phi_j(x, y, z, t)|^2 \right] \Phi_1(x, y, z, t) = i \frac{\partial \Phi_1(x, y, z, t)}{\partial t},$$

and

$$\left[ -\frac{m_r}{2} \nabla^2 + \frac{1}{2m_r} (x^2 + \alpha^2 y^2 + \lambda^2 z^2) + \sum_{j=1}^2 G_{2j} |\Phi_j(x, y, z, t)|^2 \right] \Phi_2(x, y, z, t) = i \frac{\partial \Phi_2(x, y, z, t)}{\partial t}, \quad (7)$$

where,  $g_{11} = N_1 4\pi a_{11}/a_{\text{osc}}$ ,  $g_{22} = m_r N_2 4\pi a_{22}/a_{\text{osc}}$  and  $g_{kj} = N_j 2\pi(m_1 + m_2)a_{kj}/m_2 a_{\text{osc}}$ . The TBEC system in our study is confined in a quasi-two-dimensional (quasi-2D) harmonic trap. This is achieved by considering the axial frequency of the trap,  $\omega_z$ , to be much larger than the frequencies along  $x$  and  $y$  directions, therefore,  $\lambda \gg 1$ , and to maintain radial symmetry we take  $\alpha = 1$ . This condition allows us to factorize the order parameters in the following form

$$\Phi_k(x, y, z, t) = \psi_k(x, y, t) \chi_k(z), \quad (8)$$

where,  $\chi_k(z)$  are normalized ground states of the condensates along the axial direction. Substituting Eqns. (8) in Eqns. (7), and then integrating over  $\chi_k(z)$ , we obtain the following scaled coupled GP equations in 2D

$$\left[ -\frac{1}{2} \nabla_{\perp}^2 + \frac{1}{2} (x^2 + \alpha^2 y^2) + \sum_{j=1}^2 \mathcal{G}_{1j} |\psi_j(x, y, t)|^2 \right] \times \psi_1(x, y, t) = i \frac{\partial \psi_1(x, y, t)}{\partial t},$$

and

$$\left[ -\frac{m_r}{2} \nabla_{\perp}^2 + \frac{1}{2m_r} (x^2 + \alpha^2 y^2) + \sum_{j=1}^2 \mathcal{G}_{2j} |\psi_j(x, y, t)|^2 \right] \times \psi_2(x, y, t) = i \frac{\partial \psi_2(x, y, t)}{\partial t}, \quad (9)$$

where,  $\nabla_{\perp}^2 = \partial_x^2 + \partial_y^2$ ,  $\mathcal{G}_{11} = 2N_1 \sqrt{2\pi\lambda} a_{11}/a_{\text{osc}}$ ,  $\mathcal{G}_{22} = m_r 2N_2 \sqrt{2\pi\lambda} a_{22}/a_{\text{osc}}$  and  $\mathcal{G}_{kj} = N_j(m_1 +$

$m_2)\sqrt{2\pi\lambda a_{kj}}/m_2 a_{\text{osc}}$ . With these definitions the time independent coupled GP equations are

$$\begin{aligned} & \left[ -\frac{1}{2}\nabla_{\perp}^2 + \frac{1}{2}(x^2 + \alpha^2 y^2) + \sum_{j=1}^2 \mathcal{G}_{1j} |\psi_j(x, y)|^2 \right] \psi_1(x, y) \\ &= \mu_1 \psi_1(x, y), \\ & \text{and} \\ & \left[ -\frac{m_r}{2}\nabla_{\perp}^2 + \frac{1}{2m_r}(x^2 + \alpha^2 y^2) + \sum_{j=1}^2 \mathcal{G}_{2j} |\psi_j(x, y)|^2 \right] \\ & \times \psi_2(x, y) = \mu_2 \psi_2(x, y), \end{aligned} \quad (10)$$

where,  $\mu_k$  is the chemical potential of the  $k$ th species condensate.

### A. Phase-separation

In the Thomas-Fermi (TF) limit [17, 31], depending on interaction strengths, the system can exhibit two distinct phases, miscible or immiscible (phase-separated) [32]. In the miscible phase, the condensates overlap with each other; whereas, they get spatially separated in immiscible phase. A measure to characterize these phases is the overlap integral [33]

$$\Lambda = \frac{\left[ \iint dx dy n_1(x, y) n_2(x, y) \right]^2}{\left[ \iint dx dy n_1^2(x, y) \right] \left[ \iint dx dy n_2^2(x, y) \right]}, \quad (11)$$

where,  $n_k(x, y) = |\psi_k(x, y)|^2$  is the density of the  $k$ th condensate species. A value of  $\Lambda = 1$  implies complete overlap between the condensates or the two species are completely miscible, and complete phase-separation corresponds to  $\Lambda = 0$ . The criterion for phase separation, based on the Thomas-Fermi approximation and minimization of the total energy given in Eq. (3), is  $g_{12} > \sqrt{g_{11}g_{22}}$ . It should, however, be mentioned that this condition is valid only at zero temperature, and in the absence of any topological defects. There are deviations from this criterion at  $T \neq 0$  due to the presence of thermal atoms [22]. In addition, the superflows associated with vortices in TBECs are expected to influence this criterion.

### B. Effect of vortices

Employing Madelung transformation to the order parameter  $\Psi_k(\mathbf{r}, t)$ , we can express super fluid velocity as  $\mathbf{v}_k = \hbar \nabla \theta_k / m_k$ , where,  $\theta_k(\mathbf{r}, t)$  is the phase of the order parameter. Then, the presence of a vortex in the condensate results in an additional superfluid flow (super-flow), and around it the phase of the order parameter changes by  $2\pi l$ , where  $l = \pm 1, \pm 2, \pm 3 \dots$   $l$  is the charge or vorticity of the vortex. Considering the vortex induced super-flow as purely azimuthal, the velocity of the flow at a distance  $R$  from the vor-

tex core is [34, 35]

$$\mathbf{v}_k(R) = \frac{l\hbar}{m_k R} \mathbf{e}_{\phi}. \quad (12)$$

As a consequence of this superflow, the atoms in the condensate experience a radially outward centrifugal force of magnitude

$$\mathbf{F}_k(R) = \frac{l^2 \hbar^2}{m_k R^3} \mathbf{e}_R. \quad (13)$$

From this expression, it is evident that lower atomic mass is associated with stronger force; and the quadratic dependence on  $l$  implies that the force is independent of the sign of vortex charge. Due to the centrifugal force the onset of phase-separation can be enhanced when the vortex is associated with the species that lies at the periphery at phase-separation. And, suppression when the vortex is associated with the species occupying the core at phase-separation. Thus, as mentioned earlier, the presence of vortex modifies the criterion for phase-separation. This is investigated in more detail or in a quantitative way numerically.

The stability of the vortex is dependent on the vortex charge. In a quasi-2D single species condensates, a singly charged vortex is dynamically stable, and precesses on an equidensity circular contour. But, a vortex of charge greater than unity is unstable, and spontaneously decays into multiple singly charged vortices during evolution, even in absence of dissipation and external perturbations [25, 36, 37]. In the case of a TBEC, in the immiscible domain, the vortex core in condensate of one of the species is filled by the condensate atoms of the other species [30], and the vortex is considered as coreless. Then, the superflow around the vortex in one condensate influences the other species, which results in an additional interaction among the condensates, and is responsible for a range of dynamical phenomena in TBECs [38, 39]. However, stability of a higher charge vortex during its evolution, is now dependent on the miscibility or immiscibility of the condensates together with its presence in the condensates of the species. In the TF-limit, the core size of a charge  $l$  vortex is

$$\xi_k = \frac{l}{\sqrt{2n_k(\mathcal{G}_{kk} + \mathcal{G}_{kj})}}, \quad (14)$$

where,  $n_k$  is taken to be the local TF density of the condensate at the trap center in absence of the vortex [40, 41]. Considering the larger core size and centrifugal force with higher  $l$ , the enhancement or suppression of phase-separation with a vortex in one of the species is more pronounced with higher  $l$ . However, the dynamics of the miscible-immiscible transition would exhibit complex patterns as vortex with  $l > 1$  decays to vortices with unit charge.

## III. NUMERICAL METHODS

The first step of the computations is to obtain the equilibrium solution in the miscible domain as the initial state. For

this we numerically solve Eqns. (10) in imaginary time using the split-step Crank-Nicholson method adapted for binary condensates. Furthermore, we use the numerical procedure of phase-imprinting technique to introduce a vortex of charge  $l$  by taking [24, 42] the order parameter as

$$\psi_k(x, y) = |\psi_k(x, y)| \exp \left[ il \tan^{-1} \left( \frac{y - y_0}{x - x_0} \right) \right], \quad (15)$$

where  $(x_0, y_0)$  is the location of the vortex in the condensates. To study the dynamics of phase-separation, we consider the equilibrium state solution obtained from the imaginary time propagation, and then evolve it over real time. For the present purpose, the inter-species scattering length  $a_{12}$  is adiabatically quenched from a value corresponding to the miscible phase of the TBEC to a value satisfying the phase-separation condition. The tuning of  $a_{12}$  is experimentally possible through magnetic Feshbach resonance. We investigate on the dynamics of the considered TBECs during this quench in absence and presence of a vortex in the condensates and then evolve them freely for 750ms to examine post quench dynamics of the systems.

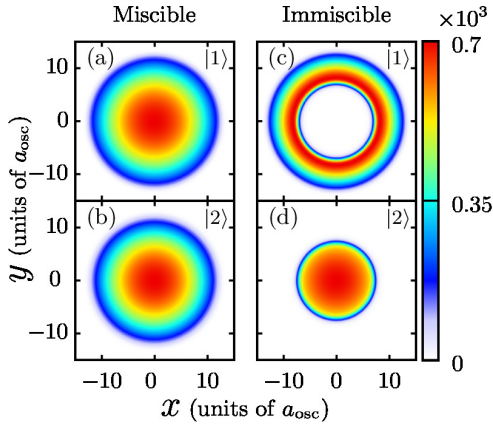


FIG. 1. (Color online) (a) and (b) show the density profiles of the Rb condensates in the two different hyperfine states when the TBEC is in miscible phase at  $a_{12} = 70a_0$ . (c) and (d) show the density profiles in the immiscible phase at  $a_{12} = 100a_0$ . In this phase, condensates of the species  $|1\rangle$  and  $|2\rangle$  become shell-condensate and core-condensate respectively. The color bar represents number density of atoms in the condensates in units of  $a_{\text{osc}}^{-2}$ , where the considered oscillator length  $a_{\text{osc}} = 1.9\mu\text{m}$ .

#### IV. RESULTS AND DISCUSSIONS

As a representative example to study the dynamics of phase-separation in the presence of a vortex, we first consider the BEC mixture in the hyperfine states  $|F = 1, m_f = -1\rangle \equiv |1\rangle$  and  $|F = 2, m_f = +1\rangle \equiv |2\rangle$  of  $^{87}\text{Rb}$ , which has been experimentally obtained to probe different static and dynamic properties of a TBEC [15, 43]. For this mixture  $m_r = 1$  as  $m_1 = m_2$ . Following the experimental realization [43] we consider a rotationally symmetric harmonic trap

with  $\omega_x = \omega_y = 2\pi \times 30.832$  Hz. And, to satisfy quasi-2D condition we consider  $\omega_z = 100.0\omega_x$  so that  $\mu_k \ll \hbar\omega_z$ , and take equal total number of atoms in the condensates as  $N_1 = N_2 = 10^5$ . The intra-species scattering lengths,  $a_{11}$  and  $a_{22}$ , are  $100.4a_0$  and  $95.44a_0$  [44], respectively, where  $a_0$  is Bohr radius. For these values, the TBEC is in the immiscible domain when  $a_{12} \geq 97.9a_0$ . To steer the TBEC from the miscible to immiscible phase, we tune  $a_{12}$  from  $70a_0$  to  $100a_0$ . As mentioned earlier, this is possible through the magnetic Feshbach resonance [16, 45, 46]. In the immiscible phase, the energetically favorable solution at equilibrium is a shell-structured geometry, in which the atoms having smaller scattering length in  $|2\rangle$  state, occupy the central region of the trap, here after referred to as the *core-condensate*. And, the atoms with the larger scattering length in  $|1\rangle$  state form a lower density shell about the core-condensate, thus, referred to as *shell-condensate*. The density profiles of the core and shell-condensate for  $a_{12} = 100a_0$  are shown in Fig. 1(c) and (d).

As an example of TBEC with unequal masses we consider  $^{87}\text{Rb}$ - $^{133}\text{Cs}$  TBEC [7], referred to as Rb-Cs TBEC for compact notation, for this mixture  $m_r \approx 0.65$ . The results for other TBECs like  $^{87}\text{Rb}$ - $^{39}\text{K}$ ,  $^{87}\text{Rb}$ - $^{23}\text{Na}$ , etc are expected to be qualitatively similar. For convenience, we label  $^{87}\text{Rb}$  and  $^{133}\text{Cs}$  to be the first and second species, respectively, and take  $N_1 = N_2 = 10^4$ . We consider this mixture in a rotationally symmetric trap with  $\omega_x = \omega_y = 2\pi \times 8$  Hz, and  $\omega_z = 40.0\omega_x$  so that  $\mu_k \ll \hbar\omega_z$ . The intra-species scattering lengths of the  $^{87}\text{Rb}$  and  $^{133}\text{Cs}$  atoms,  $a_{11}$  and  $a_{22}$ , are  $99a_0$  [45] and  $280a_0$  [47], respectively. Hence, the phase-separation condition is  $a_{12} \geq 162.8a_0$ . We drive the Rb-Cs TBEC from from the miscible to immiscible phase by varying  $a_{12}$  from  $50a_0$  to  $175a_0$  which is possible through magnetic Feshbach resonance [48]. In the immiscible phase the ground state density distribution of the system has shell-structured geometry like in the previous system. However, despite of inter-species scattering length of Cs is much larger than that of Rb, In the immiscible phase the heavier Cs atoms occupy the central region of the trap or form the core-condensate, and the lighter Rb atoms are at the edge or form the shell-condensate. This is despite the much larger intra-species scattering length of Cs atoms as this configuration tends to minimize the total energy by lowering the contribution from the trapping potential.

##### A. Dynamics of phase-separation without vortex

At initial time, the equilibrium state solution of the TBEC in Rb-hyperfine states is obtained in miscible phase by considering  $a_{12} = 70a_0$ , and the corresponding density profiles of the condensates are shown in Fig. 2(a) and (f). The condensates then have maximal overlap, and hence  $\Lambda = 0.99$ . Now, we increase  $a_{12}$  at the rate of  $0.41 a_0/\text{ms}$  [43]. The evolution of the condensate density profiles during the quench are shown in Fig. 2, and there is an increase in the total energy of the TBEC as the interaction energy increases. However, after phase-separation, when  $a_{12} > 97.9a_0$ , the overlap between the condensates becomes negligible, and therefore, the

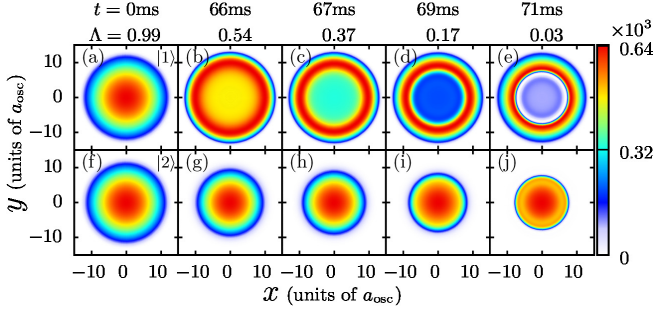


FIG. 2. (Color online) Shows the time evolution of density profiles of the Rb-condensates in  $|1\rangle$  and  $|2\rangle$  states, during the quench of  $a_{12}$ , in absence of vortices in the condensates. The first and second row show the density profiles of the condensates in  $|1\rangle$  and  $|2\rangle$  states respectively, at 0ms, 66ms, 67ms 69ms and 71ms. At these instants, the values of  $a_{12}$  are  $70a_0$ ,  $96.7a_0$ ,  $97.3a_0$ ,  $98.0a_0$  and  $98.7a_0$  respectively. Values of the overlap measure  $\Lambda$  at corresponding time instants are mentioned at the top of each column. The color bars represent number density of atoms in the condensates in units of  $a_{\text{osc}}^{-2}$  where  $a_{\text{osc}} = 1.9\mu\text{m}$ .

contribution to the total energy from the inter-species interaction is negligible. On the other hand, the higher  $a_{12}$  enhances the gradient of the density profiles at the interface, and as a consequence, the kinetic energies of the condensates are increased. This in turn enhances the total energy. In this phase, the condensate of the  $|1\rangle$  species surrounds the condensate of the  $|2\rangle$  species in shell geometry. As example, the density profiles of the condensates at 71ms, with a corresponding value of  $a_{12} = 98.7a_0$ , are shown in Fig. 2(e) and (j). From the figures, it is evident that the TBEC is in immiscible phase, and  $\Lambda = 0.04$ . We, therefore, stop quench after  $a_{12}$  attains the value of  $100a_0$  at 74ms. We then observe the free evolution of the density profiles. At later times, the condensates continue to be in this geometry while exhibiting oscillations in the overlap with frequency  $\nu \approx 185$  Hz, which is larger than the radial trap frequency  $\nu_x = 30.832$  Hz.

In a similar way, we obtain the initial equilibrium solution for the Rb-Cs TBEC in the miscible by considering  $a_{12} = 50a_0$ , and has  $\Lambda = 1.0$ . We then quench  $a_{12}$  by increasing at the rate of  $1.58 a_0/\text{ms}$  [7, 8]. The adiabaticity of the quench is verified by obtaining the stationary ground state solutions of the TBEC at the intermediate values of  $a_{12}$ . As in the previous case, the total energy of the TBEC increases with the increase of  $a_{12}$ , and the time evolution of the density profiles of the condensates are qualitatively similar. After phase-separation, when  $a_{12} > 162.8a_0$ , as mentioned earlier the Rb-condensate surrounds the Cs-condensate in a shell geometry. In this geometry, the enhanced inter-species interaction makes the size of the pancake-shaped Cs-condensate smaller than its size in the miscible phase. This reduces the trapping potential energy of the Cs-condensate; but, the enhanced density increases the interaction energy of the Cs-condensate. The quench is stopped at 79ms when  $a_{12} = 175a_0$ , and the overlap between the condensates has  $\Lambda = 0.02$ . We, then, observe the free evolution of the density profiles. At later times, the condensates continue to be in this geometry with an oscillation in the over-

lap at a frequency of  $\nu \approx 80$  Hz. Like in the previous case, this is larger than the radial trap frequency  $\nu_x = 8$  Hz.

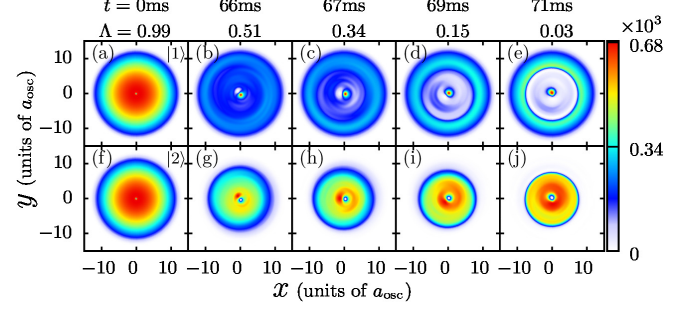


FIG. 3. (Color online) Shows the time evolution of density profiles of the Rb-condensates in  $|1\rangle$  and  $|2\rangle$  states, during the quench of  $a_{12}$ , in presence of a singly charged vortex at the center of both condensates. The first and second row show the density profiles of the condensates in  $|1\rangle$  and  $|2\rangle$  states respectively, at 0ms, 66ms, 67ms 69ms and 71ms. At these instants, the values of  $a_{12}$  are  $70a_0$ ,  $96.7a_0$ ,  $97.3a_0$ ,  $98.0a_0$  and  $98.7a_0$  respectively. Values of the overlap measure  $\Lambda$  at corresponding time instants are mentioned at the top of each column. The color bars represent number density of atoms in the condensates in units of  $a_{\text{osc}}^{-2}$  where  $a_{\text{osc}} = 1.9\mu\text{m}$ .

## B. Presence of singly-charged vortex

### 1. Vortices in both the condensates

To examine the dynamics of the phase separation in the presence of a vortex in the Rb hyperfine TBEC, we consider the equilibrium state with the same set of parameters as previous. But, now we imprint singly charged vortices at the center of both the species. In experiments, this may be achieved by employing topological phase imprinting techniques [24]. After obtaining the equilibrium solution, like in the previous case, we quench  $a_{12}$ , to induce miscibility-immiscibility phase transition in the system. During the course of the evolution the vortices are displaced from the center and start to precess, and the density profiles are as shown in Fig. 3. During the quench there is an enhancement of the miscible-immiscible transition, which is evident from the trend in the value of  $\Lambda$  as shown in Fig. 4. From the figure there is a manifest faster decrease in  $\Lambda$  when vortices are present in both the species.

For the Rb-Cs as well we follow the same protocol of imprinting vortices in both the species, and quenching  $a_{12}$  at the same rate as it was done when the vortex was absent. Among the two condensates, due to the shorter healing length, the vortex core size in the Cs-condensate is smaller than in Rb. Here, the shorter healing length of Cs is on account of its larger mass and scattering length. Unlike in the case of the Rb-hyperfine TBEC, the vortices in the Rb-Cs TBEC remain at the center and the core size of the vortex in Rb-condensate increases. Following the values of  $\Lambda$  during time evolution, as shown in Fig. 6, it is evident that there is an enhancement in the



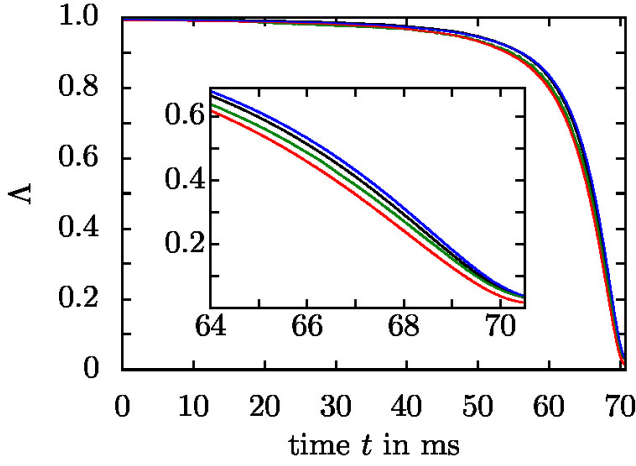


FIG. 4. (Color online) Shows the variation of the overlap measure  $\Lambda$  with time as  $a_{12}$  of the TBEC in Rb-hyperfine states quenched from  $70a_0$  to  $100a_0$ . The black curve shows this variation in absence of defects in the condensates, the green curve shows it when a singly charged vortex is present at the center of both condensates; whereas, the red curve shows the variation when the vortex is present only in the condensate of species  $|1\rangle$  (shell-condensate) but not in the condensate of species  $|2\rangle$  (core-condensate), and the blue curve shows the variation when the vortex is present only in the species  $|2\rangle$  but not in the condensate of species  $|1\rangle$ .

miscible-immiscible transition. To investigate further we imprint vortices with opposite charges, and find that the trend in the miscible-immiscible transition is independent of the sign of the vortex charges. In other words, it is the presence of the superflow which influences the onset of the phase-separation, but the direction of the superflow does not impact on the transition. As evident from the comparison of the trends in Fig. 4 and Fig. 6, the effect of the vortices is more pronounced in the case of Rb-Cs. This is on account of the difference in the masses and relative intra-species scattering lengths.

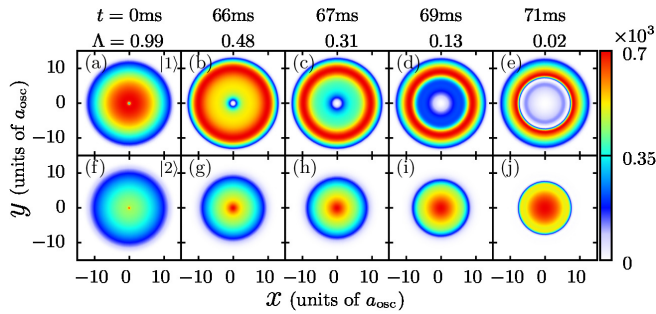


FIG. 5. (Color online) Shows the time evolution of density profiles of the Rb-condensates in  $|1\rangle$  and  $|2\rangle$  states, during the quench of  $a_{12}$ , in presence of a singly charged vortex at the center of the shell-condensate. The first and second row show the density profiles of the condensates in  $|1\rangle$  and  $|2\rangle$  states respectively, at 0ms, 66ms, 67ms, 69ms and 71ms. At these instants, the values of  $a_{12}$  are  $70a_0$ ,  $96.7a_0$ ,  $97.3a_0$ ,  $98.0a_0$  and  $98.7a_0$  respectively. Values of the overlap measure  $\Lambda$  at corresponding time instants are mentioned at the top of each column. The color bars represent number density of atoms in the condensates in units of  $a_{osc}^{-2}$  where  $a_{osc} = 1.9\mu\text{m}$ .

## 2. Vortex in shell-condensate

To study the miscible-immiscible transition when vortex is present in only one of the species in Rb-hyperfine TBEC, we first examine the evolution of the TBEC with a vortex present only in the condensate of species  $|1\rangle$ . Like in the previous cases, we obtain the initial state of the system in the miscible phase, and then, imprint a singly charged vortex at the center of the condensate of species  $|1\rangle$ . In experiments the generation of a vortex in either the condensate of Rb hyperfine TBEC was demonstrated by M. R. Matthews et al. [30]. The initial density profiles of the condensates are as shown in Fig. 5(a) and (f). As to be expected the vortex is core-less, that is, condensate of  $|2\rangle$  occupies the core of the vortex. Now, to observe the miscible-immiscible transition we quench  $a_{12}$ , and the density profiles during the quench are shown in Fig. 5. As the value of  $a_{12}$  is increased, the core size of the vortex increases, and hence, larger number of atoms of species  $|2\rangle$  occupy the vortex core. Since, the vortex is imprinted with the shell-condensate, as shown in Fig. 1(c) and (d), there is an enhancement in the miscibility-immiscibility transition due to the centrifugal force associated with the vortex induced superflow. The enhancement is evident from the trend in  $\Lambda$  as shown in Fig. 4, and the effect is more pronounced compared to the presence of vortices in both the species.

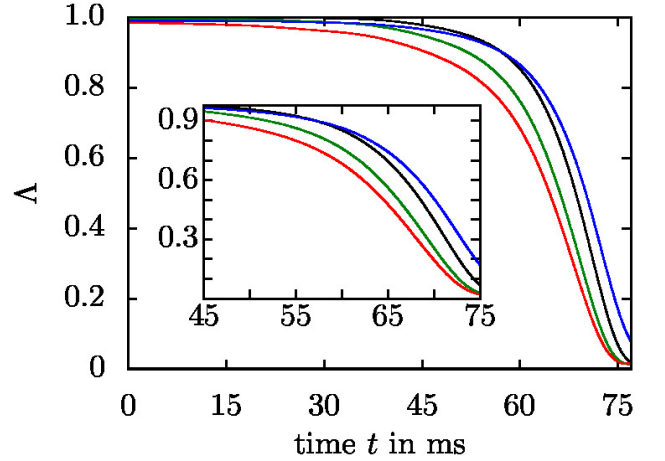


FIG. 6. (Color online) Shows the variation of the overlap measure  $\Lambda$  with time as  $a_{12}$  of the Rb-Cs TBEC is quenched from  $50a_0$  to  $175a_0$ . The black curve shows this variation in absence of defects in the condensates, the green curve shows it when a singly charged vortex is present at the center of both condensates; whereas, the red curve shows the variation when the vortex is present only in the Rb-condensate (shell-condensate) but not in the Cs-condensate (core-condensate), and the blue curve shows the variation when the vortex is present only in the Cs-condensate but not in the Rb-condensate.

Another important observation is, vortex with higher charge leads to larger enhancement in the miscible-immiscible transition. This is to expected since, as discussed earlier, the centrifugal force is proportional to  $l^2$ , where  $l$  is the charge of the vortex. In the present case, there is an important observation, the vortices of higher charges are stable through the quench, and significant later times as well. This is in contrast to the

case of single species condensates, where vortices of higher charges are dynamically unstable and decays in singly charged vortices with short time scales. The stability of a higher charge vortex in TBEC may be attributed to the immiscibility of the TBEC. Because, if the vortex decays to multiple vortices of lower charges it would increase the inter-species interaction energy due to the filling of the vortex cores. In short, TBEC supports higher charge vortex in the immiscible phase when the vortex is present in the shell-condensate.

Similarly, for the Rb-Cs TBEC, we again obtain the initial equilibrium solution in the miscible phase, and a singly charged vortex imprinted at the center of the Rb-condensate. It is to be mentioned here that, the Rb despite of having smaller atomic scattering is the shell-condensate due to the smaller mass. In this case, the quench of  $a_{12}$  leads to qualitatively similar results as in Rb-hyperfine TBEC. That is, the core size of the vortex increases during the quench, and the vortex induced superflow in the Rb-condensate enhances the phase-separation. This evident from the trends in the values of  $\Lambda$  shown in Fig. 6.

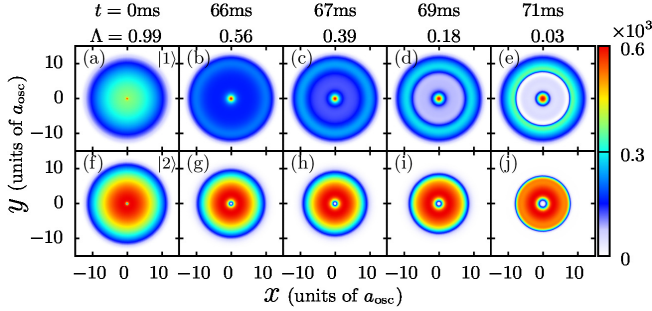


FIG. 7. (Color online) Shows the time evolution of density profiles of the Rb-condensates in  $|1\rangle$  and  $|2\rangle$  states, during the quench of  $a_{12}$ , in presence of a singly charged vortex at the center of the core-condensate. The first and second row show the density profiles of the condensates in  $|1\rangle$  and  $|2\rangle$  states respectively, at 0ms, 66ms, 67ms 69ms and 71ms. At these instants, the values of  $a_{12}$  are  $70a_0$ ,  $96.7a_0$ ,  $97.3a_0$ ,  $98.0a_0$  and  $98.7a_0$  respectively. Values of the overlap measure  $\Lambda$  at corresponding time instants are mentioned at the top of each column. The color bars represent number density of atoms in the condensates in units of  $a_{osc}^{-2}$  where  $a_{osc} = 1.9\mu\text{m}$ .

### 3. Vortex in core-condensate

In this section we examine the dynamics of phase-separation when a vortex is present in the core-condensate. For this, like in the previous case, the initial state of the Rb-hyperfine TBEC is in the miscible phase, and a singly charged vortex is imprinted at the center of the  $|2\rangle$  condensate. The initial density profiles of the condensates are as shown in Fig. 7(a) and (f). We then quench the system by increasing  $a_{12}$  to drive the system to immiscible phase. The density profiles of the condensates at different times during the quench are shown in Fig. 7. During this evolution, the core size of the vortex increases, and an increasing number of atoms from species  $|1\rangle$  occupy the vortex core. Thus, in the immiscible phase of

the TBEC, the density profile of the condensate of the species  $|1\rangle$  acquires a *bull's eye* structure as shown in Fig. 7(e). From the trend in  $\Lambda$ , shown in Fig. 4, it is evident that there is a suppression in phase-separation of the TBEC as the decrease in  $\Lambda$  slower than the previous cases. The radially outward centrifugal force arising from the vortex leads to a larger radial size of the  $|2\rangle$  condensate, and thus the atoms of  $|1\rangle$  require larger inter-species repulsion energy to be the shell-condensate at phase separation. In other words, the vortex induced superflow in the core-condensate is responsible for suppression of phase separation. From similar computations, we also find the same trend in the Rb-Cs TBEC. In fact, the effect of suppression is more pronounced in this system, this is discernible by comparing the trends in the values of  $\Lambda$  plotted in Fig. 4 and 6.

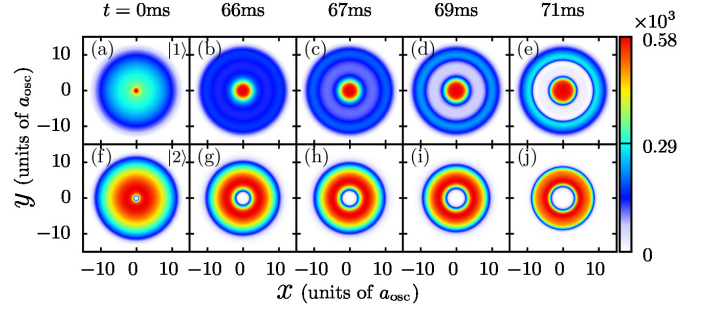


FIG. 8. (Color online) Shows time evolution of the density profiles of the TBEC in Rb-hyperfine states during the quench of  $a_{12}$  in presence of a quadruply charged vortex at the center of the condensate of species  $|2\rangle$ . The color bars represent number density of atoms in the condensate in units of  $a_{osc}^{-2}$  where  $a_{osc} = 1.9\mu\text{m}$ .

### C. Higher charge vortex

We now examine the dynamics of phase separation in presence of a higher charge vortex, in particular with core-condensates. In experiments, doubly and quadruply charged vortices are generated using topological phase-imprinting technique [24, 25]. The cases of vortices in both the condensates or only with shell condensate are qualitatively similar to the cases of singly charged vortices. Like in the previous cases, we obtain initial equilibrium state of the Rb-hyperfine TBEC in the miscible phase, but with a quadruply charged vortex imprinted at the center of species  $|2\rangle$  or the core condensate. Then, we quench  $a_{12}$  from  $70a_0$  to  $100a_0$  for miscibility-immiscibility phase transition in the TBEC. During the quench the core size of the vortex increases, and it gets filled with the atoms of species  $|1\rangle$  as shown in Fig. 8. Hence, in the immiscible phase, the density profile of the condensate of species  $|1\rangle$  has bull's eye structure with a higher density core-region and a lower density ring outside the condensate of species  $|2\rangle$ . So, most of the atoms of species  $|1\rangle$  occupy the core region of the vortex, and is the consequence of larger core-size associated with the higher charged vortex. Thus, the overall configuration has the density profile of the species  $|2\rangle$  resembling the geometry shell-condensate. In

other words, the presence of quadruply charged vortex forces the species with lower intra-species interaction to occupy the edges, and the species with higher intra-species interaction to occupy the core region by filling the vortex core. This can be referred to as the vortex induced partial position reversal at phase-separation. There is complete position reversal when we consider a vortex with charge higher than  $l = 4$ .

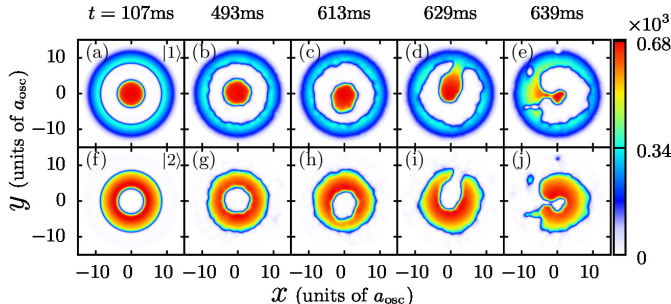


FIG. 9. (Color online) Shows post quench free dynamics of the phase-separated TBEC in Rb-hyperfine states in presence of a quadruply charged vortex at the center of the condensate of species  $|2\rangle$ . The color bars represent number density of atoms in the condensate in units of  $a_{\text{osc}}^{-2}$ , where  $a_{\text{osc}} = 1.9\mu\text{m}$ .

The position reversed geometry is important to study as it provides a framework to investigate the dynamics related to Rayleigh-Taylor instability (RTI) in TBECs [1, 49]. The instability sets in as the species initially occupying the core region is driven to the edge in the presence of the higher charged vortex when  $a_{12}$  is quenched. In the case of quadruply charged vortex RTI is not observed, and the vortex induced azimuthal super-flow in the species  $|2\rangle$  is responsible for inhibition of RTI at the interface of the condensates. This follows from the general result of suppression of RTI by the pressure gradient in the radial direction [50], in the present case arising from the Coriolis force acting on atoms of species  $|2\rangle$ . In a related work, the suppression of RTI at the interface of rotating, immiscible, inviscid classical fluids has been reported [51]. Although RTI doesn't occur, the system exhibits a rich dynamics associated with the precession motion of the vortex during the post quench free evolution of the TBEC as shown in Fig. 9. The condensates continue to be in the bull's eye and shell geometry respectively for sufficiently long time till  $\approx 500\text{ms}$ . However, at later times, there is instability at the interface arising from the shear at the interface due to the superflow and decay of the higher charged vortex. The density

profiles of the TBEC at selected times during this later evolution are evident from the density plots in Fig. 9. We obtain qualitatively similar results for Rb-Cs TBEC in the presence of quadruply charged vortex in the Cs-condensate. Hence, in this case, as the TBEC is quenched to immiscible phase, the Rb-condensate takes the bull's eye structure, and the density profile of the Cs-condensate resembles with shell-condensate.

## V. CONCLUSIONS

In presence of singly charged vortex in the shell-condensates of the TBECs, the centrifugal force associated with the vortex induced azimuthal superflow enhances the miscibility-immiscibility phase-separation. The same force resulting from the vortex induced superflow in the core-condensates suppresses the phase-separation. However, there is a net enhancement when singly charged vortices are present in both of the species. Compared to the Rb hyperfine TBEC, in Rb-Cs TBEC the centrifugal force experienced by Rb atoms is stronger. Hence, the enhancement or suppression of phase-separation due to the presence of vortex is more prominent in Rb-Cs TBEC. The quadratic dependence of the centrifugal force on the vortex charge, ensures the obtained results are independent on the sense of circulation of the super-flows. The results from the Rb-Cs TBEC are generic to the TBECs in which the species have considerable mass difference, and different intra-species interactions. Similarly, the results of the Rb hyperfine TBEC is generic to other TBEC of two hyperfine states, isotopes of the same elements or different atoms with nearly equal mass and scattering length. Thus, the cases considered is representative of other TBEC. In presence of a vortex of quadruply charged vortex in the core-condensate, a phase-separated state of the TBECs is obtained in which the components of the TBECs partially swap their positions in the shell-structured geometry in comparison with the case when the vortex is absent. From the post quench free dynamics, at later times there is an instability at the interface and decay of the quadruply charged vortex.

## ACKNOWLEDGMENTS

We thank S. Pal, K. Suthar and R. Bai for useful discussions. The results presented in this paper are based on the computations using Vikram-100, the 100TFLOP HPC Cluster at Physical Research Laboratory, Ahmedabad, India.

[1] K. Sasaki, N. Suzuki, D. Akamatsu, and H. Saito, Phys. Rev. A **80**, 063611 (2009).  
[2] D. Kobyakov, V. Bychkov, E. Lundh, A. Bezett, V. Akkerman, and M. Marklund, Phys. Rev. A **83**, 043623 (2011).  
[3] T. Kadokura, T. Aioi, K. Sasaki, T. Kishimoto, and H. Saito, Phys. Rev. A **85**, 013602 (2012).  
[4] J. Sabbatini, W. H. Zurek, and M. J. Davis, Phys. Rev. Lett. **107**, 230402 (2011).

[5] G. Modugno, M. Modugno, F. Riboli, G. Roati, and M. Inguscio, Phys. Rev. Lett. **89**, 190404 (2002).  
[6] G. Thalhammer, G. Barontini, L. De Sarlo, J. Catani, F. Minardi, and M. Inguscio, Phys. Rev. Lett. **100**, 210402 (2008).  
[7] D. J. McCarron, H. W. Cho, D. L. Jenkin, M. P. Köppinger, and S. L. Cornish, Phys. Rev. A **84**, 011603(R) (2011).  
[8] A. D. Lercher, T. Takekoshi, M. Debatin, B. Schuster, R. Rameshan, F. Ferlaino, R. Grimm, and H. C. Nägerl, Eur. Phys. J. D



- 65**, 3 (2011).
- [9] B. Pasquiou, A. Bayerle, S. M. Tzanova, S. Stellmer, J. Szczepkowski, M. Parigger, R. Grimm, and F. Schreck, *Phys. Rev. A* **88**, 023601 (2013).
  - [10] L. Wacker, N. B. Jørgensen, D. Birkmose, R. Horchani, W. Ertmer, C. Klempt, N. Winter, J. Sherson, and J. J. Arlt, *Phys. Rev. A* **92**, 053602 (2015).
  - [11] F. Wang, X. Li, D. Xiong, and D. Wang, *J. Phys. B* **49**, 015302 (2016).
  - [12] S. B. Papp, J. M. Pino, and C. E. Wieman, *Phys. Rev. Lett.* **101**, 040402 (2008).
  - [13] S. Sugawa, R. Yamazaki, S. Taie, and Y. Takahashi, *Phys. Rev. A* **84**, 011610 (2011).
  - [14] C. J. Myatt, E. A. Burt, R. W. Ghrist, E. A. Cornell, and C. E. Wieman, *Phys. Rev. Lett.* **78**, 586 (1997).
  - [15] D. S. Hall, M. R. Matthews, J. R. Ensher, C. E. Wieman, and E. A. Cornell, *Phys. Rev. Lett.* **81**, 1539 (1998).
  - [16] S. Tojo, Y. Taguchi, Y. Masuyama, T. Hayashi, H. Saito, and T. Hirano, *Phys. Rev. A* **82**, 033609 (2010).
  - [17] T.-L. Ho and V. B. Shenoy, *Phys. Rev. Lett.* **77**, 3276 (1996).
  - [18] S. Gautam and D. Angom, *J. Phys. B* **44**, 025302 (2011).
  - [19] R. Navarro, R. Carretero-González, and P. G. Kevrekidis, *Phys. Rev. A* **80**, 023613 (2009).
  - [20] R. W. Pattinson, T. P. Billam, S. A. Gardiner, D. J. McCarron, H. W. Cho, S. L. Cornish, N. G. Parker, and N. P. Proukakis, *Phys. Rev. A* **87**, 013625 (2013).
  - [21] K. L. Lee, N. B. Jørgensen, I.-K. Liu, L. Wacker, J. J. Arlt, and N. P. Proukakis, *Phys. Rev. A* **94**, 013602 (2016).
  - [22] A. Roy and D. Angom, *Phys. Rev. A* **92**, 011601(R) (2015).
  - [23] L. Wen, W. M. Liu, Y. Cai, J. M. Zhang, and J. Hu, *Phys. Rev. A* **85**, 043602 (2012).
  - [24] A. E. Leanhardt, A. Görlitz, A. P. Chikkatur, D. Kielpinski, Y. Shin, D. E. Pritchard, and W. Ketterle, *Phys. Rev. Lett.* **89**, 190403 (2002).
  - [25] Y. Kawaguchi and T. Ohmi, *Phys. Rev. A* **70**, 043610 (2004).
  - [26] K.-P. Marzlin, W. Zhang, and E. M. Wright, *Phys. Rev. Lett.* **79**, 4728 (1997).
  - [27] K.-P. Marzlin and W. Zhang, *Phys. Rev. A* **57**, 3801 (1998).
  - [28] K.-P. Marzlin and W. Zhang, *Phys. Rev. A* **57**, 4761 (1998).
  - [29] R. J. Marshall, G. H. C. New, K. Burnett, and S. Choi, *Phys. Rev. A* **59**, 2085 (1999).
  - [30] M. R. Matthews, B. P. Anderson, P. C. Haljan, D. S. Hall, C. E. Wieman, and E. A. Cornell, *Phys. Rev. Lett.* **83**, 2498 (1999).
  - [31] G. Baym and C. J. Pethick, *Phys. Rev. Lett.* **76**, 6 (1996).
  - [32] M. Trippenbach, K. Gral, K. Rzazewski, B. Malomed, and Y. B. Band, *J. Phys. B* **33**, 4017 (2000).
  - [33] P. Jain and M. Boninsegni, *Phys. Rev. A* **83**, 023602 (2011).
  - [34] C. Pethick and H. Smith, *Bose-Einstein Condensation in Dilute Gases* (Cambridge University Press, New York, 2008).
  - [35] M. Ueda, *Fundamentals and New Frontiers of Bose-Einstein Condensation* (World Scientific, Singapore, 2010).
  - [36] H. Pu, C. K. Law, J. H. Eberly, and N. P. Bigelow, *Phys. Rev. A* **59**, 1533 (1999).
  - [37] Y. Shin, M. Saba, M. Vengalattore, T. A. Pasquini, C. Sanner, A. E. Leanhardt, M. Prentiss, D. E. Pritchard, and W. Ketterle, *Phys. Rev. Lett.* **93**, 160406 (2004).
  - [38] J. J. García-Ripoll and V. M. Pérez-García, *Phys. Rev. Lett.* **84**, 4264 (2000).
  - [39] P. Öhberg and L. Santos, *Phys. Rev. A* **66**, 013616 (2002).
  - [40] S. Ishino, M. Tsubota, and H. Takeuchi, *Phys. Rev. A* **88**, 063617 (2013).
  - [41] S. Gautam, P. Muruganandam, and D. Angom, *Phys. Lett. A* **377**, 378 (2013).
  - [42] L. Dobrek, M. Gajda, M. Lewenstein, K. Sengstock, G. Birkel, and W. Ertmer, *Phys. Rev. A* **60**, R3381 (1999).
  - [43] K. M. Mertes, J. W. Merrill, R. Carretero-González, D. J. Frantzeskakis, P. G. Kevrekidis, and D. S. Hall, *Phys. Rev. Lett.* **99**, 190402 (2007).
  - [44] M. Egorov, B. Opanchuk, P. Drummond, B. V. Hall, P. Hannaford, and A. I. Sidorov, *Phys. Rev. A* **87**, 053614 (2013).
  - [45] A. Marte, T. Volz, J. Schuster, S. Dürr, G. Rempe, E. G. M. van Kempen, and B. J. Verhaar, *Phys. Rev. Lett.* **89**, 283202 (2002).
  - [46] M. Erhard, H. Schmaljohann, J. Kronjäger, K. Bongs, and K. Sengstock, *Phys. Rev. A* **69**, 032705 (2004).
  - [47] C. Chin, V. Vuletić, A. J. Kerman, S. Chu, E. Tiesinga, P. J. Leo, and C. J. Williams, *Phys. Rev. A* **70**, 032701 (2004).
  - [48] K. Pilch, A. D. Lange, A. Prantner, G. Kerner, F. Ferlaino, H.-C. Nägerl, and R. Grimm, *Phys. Rev. A* **79**, 042718 (2009).
  - [49] S. Gautam and D. Angom, *Phys. Rev. A* **81**, 053616 (2010).
  - [50] S. Chandrasekhar, *Hydrodynamic and Hydromagnetic Stability*, Dover Books on Physics (Dover Publications, New York, 2013).
  - [51] J. J. Tao, X. T. He, W. H. Ye, and F. H. Busse, *Phys. Rev. E* **87**, 013001 (2013).